

A flexible islanding identification technique for PV based grid-tied systems

Praveen Raj Rajaswamy Sarojam¹, Joseph Sarojini Xavier²

¹Department of Electrical and Electronics Engineering, Mar Baselios College of Engineering and Technology, Nalanchira, India

²Department of Electrical Engineering, College of Engineering, Trivandrum, India

Article Info

Article history:

Received Jul 7, 2023

Revised Aug 25, 2023

Accepted Sep 14, 2023

Keywords:

ABRPP

Grid integration

Hybrid islanding identification scheme

Non-detection zone

Quality factor

SWMA

ABSTRACT

The phenomenon of islanding, which occurs in grid integrated distributed generators (DGs), poses significant challenges and potential risks for customers, utility providers, and operational personnel. Detecting islanding quickly and accurately is crucial. The issues related to the conventional islanding methods paved the way in developing a hybrid islanding identification scheme. The developed method achieves accurate results within a reduced time span of 30 ms. The hybrid technique combines the passive method of sliding window based moving average (SWMA) for faster detection and the active method of asymmetrical bilateral reactive power perturbation (ABRPP) for improved precision. The developed hybrid method is simulated and tested using MATLAB/Simulink 2023a. It undergoes testing under various load conditions, including small and large power mismatches between DG generation and local load demand, as well as different load quality factors (Q_F). Additionally, the hybrid algorithm demonstrates no nuisance tripping when subjected to different load switching conditions such as capacitor switching, motor load switching, and nonlinear load switching. A comparison with existing islanding detection methods confirms the accuracy and speed of the proposed method in identifying islanding conditions.

This is an open access article under the [CC BY-SA](https://creativecommons.org/licenses/by-sa/4.0/) license.



Corresponding Author:

Praveen Raj Rajaswamy Sarojam

Department of Electrical and Electronics Engineering, Mar Baselios College of Engineering and Technology

Mar Ivanios Vidyannagar, P.O, Nalanchira, Thiruvananthapuram, Kerala 695015, India

Email: india.praveenraj@gmail.com

1. INTRODUCTION

In the present decade the renewable energy source dependent distributed generation (DG) systems have significant contribution to the power sector [1]. The progress in the emerging technology of power semiconductor devices and its control methods has enhanced the flexibility of integrating DGs with the traditional grid [2]. The penetration of DGs into the existing power system, improves the serviceability and reliability of the system [3], [4]. However, the process of synchronizing DGs with the grid presents certain constraints, such as the islanding scenarios, which can impede the effectiveness of DG synchronization. Islanding refers to a situation where a DG continues to provide power to a section of the power system even when the main grid is in-operative. Identification of Islanding is a matter of grave concern as it poses threats to equipment as well as the working people. According to the IEEE standard 1547 cited in [5], it is obligatory for a DG system to cease power supply to the grid within a maximum of 2 seconds following the occurrence of islanding. Several islanding identification schemes (IIS) have been introduced in the literature, to identify the islanding scenario [6]. The IIS can be broadly categorized as remotely controlled and locally controlled schemes [7]. The remotely controlled schemes primarily rely on the transmitting and receiving of

communication signals between the utility grid and the DG points. Some examples of remotely controlled IIS include power line carrier communication (PLCC) based schemes [8] and SCADA based schemes [9]. Though the non-detection zone (NDZ) of these schemes is noteworthy, they are very expensive and their reliability is contingent upon the speed of communication devices and signals involved. The locally controlled IIS encompass passive, active, hybrid (a combination of passive and active methods), and intelligent based methods. Passive IIS rely on the measurement of point of common coupling (PCC) parameters such as over voltage (OV), under voltage (UV), over frequency (OF), under frequency (UF) [10], rate of change of frequency (ROCOF) [11], voltage unbalance (VU) [12], voltage/current total harmonic distortion (THD) [13]. These methods do not cause any power quality issues, but are quick to respond, easy to implement, and cost-effective. Raising PCC parameter thresholds, increases the NDZ, yet excessively low settings can cause nuisance tripping. Additionally, as grid power to local loads nears zero, passive IIS struggles to detect islanding state due to minor PCC parameter deviations during such scenarios. As a result, there arose a need for the development of active IIS.

Active IIS intentionally introduces perturbations from DG inverters to the grid and local load at PCC. While the grids low impedance absorbs these perturbations in a grid integrated DG (GIDG), islanding shifts PCC parameters past thresholds, activating relays for tripping. Some examples of active IIS are harmonic injection [14], sandia frequency/voltage shift (SFS, SVS) [15], active power and reactive power variation [16], [17], and impedance measurement [18]. While these methods decrease NDZ, they compromise power quality [19] due to the injected perturbations. Active techniques require more time for islanding detection, to observe the response of injected perturbation. Blending passive and active IISs in a hybrid approach capitalizes on their respective benefits but also aggregates the limitations tied to each method. Some of the hybrid methods are voltage unbalance and SFS [20], rate of change of frequency and harmonic injection [21], rate of change of voltage (ROCOV) and active/reactive power disturbance [22]–[24], ROCOF and impedance measurement (IM) [25]–[27]. The hybrid method detects faster than passive but slower than active approaches. However, it brings extra drawbacks, including perturbation impact and conflicts among front-end DG inverters. From summarized literature in Table 1, it has been identified that passive methods offer quicker detection with minor power quality impact but a larger NDZ. To curtail the NDZ, passive thresholds are reduced, risking nuisance tripping. Active methods mitigate this NDZ, but affects the power quality. Yet, they rely on post-perturbation system response, causing delay in detection strategies. Existing hybrid methods lack the desirable quick detection time of passive methods. Thus, a hybrid IIS with reduced NDZ and detection time is to be formulated. Leveraging passive traits, the method should independently operate by utilizing initial cycle features upon islanding. Active perturbations can further enhance these traits for its reliability. The following factors must be taken into account when developing an effective hybrid islanding detecting strategy.

- The passive scheme must autonomously identify islanding, avoiding reliance on the response of the active method, in order to reduce the detection time.
- By lowering the NDZ, the active approach ought to increase its reliability.
- It must be capable of detecting islanding events under all possible operational circumstances.
- There should not be any malfunction in response to disturbances other than islanding.
- The detection strategy should be easy to implement, not only for a new system but also for existing systems.

Table 1. Summary of certain conventional passive, active, and hybrid methods

Traits	Passive Methods				Active Methods				Hybrid Methods			
	[10]	[11]	[12]	[13]	[14]	[15]	[16]	[18]	[20]	[21]	[22]	[25]
NDZ	Large	Small	Large	Higher QF-larger NDZ	Very small	Very small	small	small	Same as SFS	Same as Harmonic injection	Same as Variation of power	small
Detection Time	4ms-2s	24ms	53ms	45ms	Few ms	0.5s - 1s	0.3s - 0.75s	0.77s - 0.95s	0.15s - 0.21s	0.2s	0.5s	0.216s
Limitations	Power mismatch between DG and Load is desired	suitable for highly fluctuating loads. Power mismatch is desired	As pf comes close to unity, error increases	Grid disturbance causes error in detection	Affects PQ slightly	Affects PQ slightly, Needs strong grid	Affects PQ	Threshold setting difficult, Affects PQ	Affects PQ slightly	Same as Harmonic injection	Affects PQ during injection	Same as IM

Therefore, a hybrid method which harvests the minimum NDZ of its active method without losing the quick response characteristics of the passive method is formulated. The proposed hybrid technique, employs sliding window based moving average computation (SWMA) [28], [29] algorithm for passive

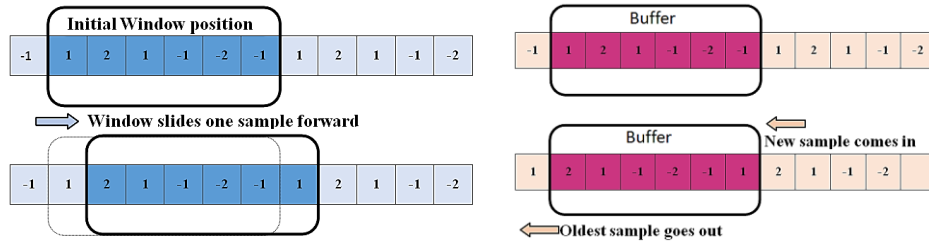


Figure 2. Working of the sliding window

Typically, the average of a symmetrical periodic wave is computed over half a period. But, in this approach, it is calculated across one fundamental time period (0.02 seconds) corresponding to the nominal frequency. In Figure 3, during GIDG operation, window 1 exhibits equal positive and negative areas, yielding a zero average DG voltage for one period. In contrast, islanding causes frequency deviations, as shown in windows 2 and 3, resulting in a positive average. SWMA approach is illustrated in Figure 4 with a sampling frequency of 100 kHz and its discrete fundamental period is around 2000 samples (1000 positive and negative each). To maintain zero discrete mean in GIDG operation, the window should align with the fundamental period. Once the window is full, the moving average is computed. The mean value is recalculated by shifting the window with one sample. During grid’s absence, any deviation in DG frequency leads to a non-zero positive mean.

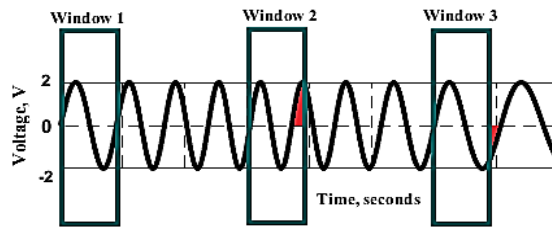


Figure 3. Moving average during frequency deviation

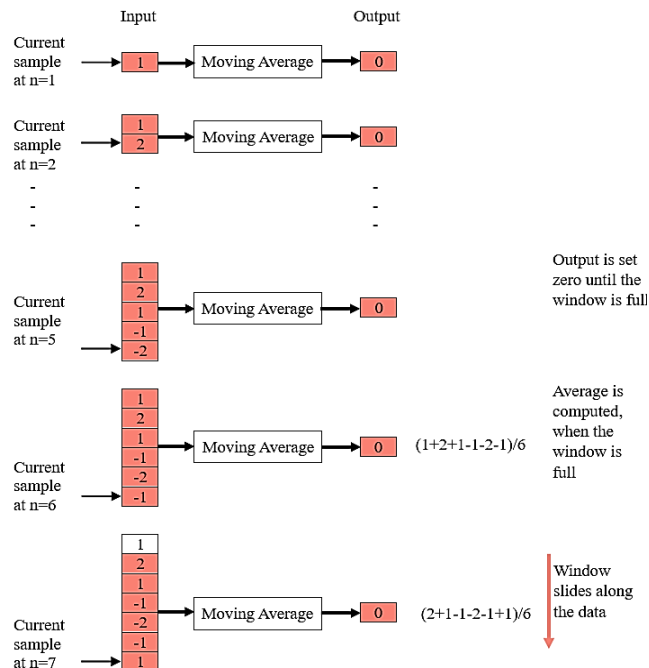


Figure 4. Sliding window based moving average computation

IEEE standard 1547 permits DG voltage and frequency deviations within specific ranges. Voltage ranges from 0.88 pu to 1.1 pu, with a lower limit of 0.88 pu. Frequency ranges between 49.5 to 50.5 Hz, with a lower limit of 49.5 Hz. The average voltage values are calculated using in (1).

$$V_a(y) = \frac{1}{N} \sum_{i=1}^{N-1} V(y) \quad (1)$$

Where N represents the number of sampled data at each position of the sliding window. The magnitude of the average voltage in a window depends on the window position. In order to overcome this drawback, cumulative average voltage (CAV) is calculated using in (2) for each window.

$$V_{cuma} = \sum_{i=1}^{N-1} \text{mod} V_a(y) \quad (2)$$

The cumulative average voltage is computed at the end of each sliding window. The cumulative voltage index is computed as (3):

$$K_{\Psi} = \Delta V_{pu} V_{cuma} \quad (3)$$

where, ΔV_{pu} is the change in DG voltage represented in pu. The threshold value K_v is computed as (4)-(6):

$$K_v = \text{mod}(\Delta V_{pu}) N V_a \quad (4)$$

$$K_v = \text{mod}(\Delta V_{pu}) N \frac{1}{N} \text{mod} \sum_{i=1}^{n-1} V(y) \quad (5)$$

$$K_v = \text{mod}(\Delta V_{pu}) \text{mod} \sum_{y=1}^{n-1} V(y) \quad (6)$$

where, n represents the number of samples pertaining to the lower frequency $f=49.5$ Hz.

$$n = \frac{49.5}{50} \times N = 1980 \text{ samples}$$

$$\Delta V = 1 \text{ pu} - 0.88 \text{ pu} = 0.12 \text{ pu}$$

The voltage signal in the continuous domain is considered as, $V(t) = V_m \sin(\omega t)$, after the sampling process, the voltage signal in the discrete domain is obtained as,

$$V(y) = [V(1), V(2), V(3), \dots, V(n) \dots, V(N)]$$

the threshold value is calculated in MATLAB, and is obtained as $K_v = 0.38 \text{ pu}$, in continuous domain, the threshold value can be computed as (7) and (8):

$$K_v = \text{mod}(\Delta V_{pu}) N V_a \quad (7)$$

$$K_v = \frac{\text{mod}(\Delta V_{pu}) N}{2\pi} \int_0^{\theta} V_m \sin \theta d\theta \quad (8)$$

θ is the angle pertaining to $f=49.5$ Hz

$$\theta = \frac{49.5}{50} \times 2\pi = 1.98\pi \text{ rad}$$

$\Delta V = 1 \text{ pu} - 0.88 \text{ pu} = 0.12 \text{ pu}$, $V_m = 1 \text{ pu}$, $N=2000$ samples in the sliding window, $K_v = 0.38 \text{ pu}$. The CAV is compared with the threshold value, to identify islanding state, as illustrated in the Figure 5.

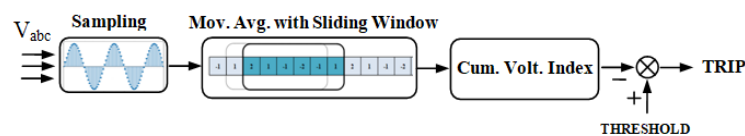


Figure 5. Block schematic of SWMA method

2.2. Bi-lateral reactive power perturbation

Bilateral reactive power injection [22] creates the PCC frequency to vary in the absence of grid. But in the grid interfaced operation, due to the presence of low impedance grid, the DG inverter frequency adheres to the nominal value. During grid tied mode, the voltage at the PCC (V_C) and the grid voltage (V_P), are equal. The analysis of the Bi-lateral reactive power perturbation is presented in [22].

The NDZ in this method is denoted as NDZ (+) when the reactive power injected at the PCC from the DG is Q (+) and as NDZ (-) when the reactive power injected at the PCC from the DG is Q (-). Minimizing the overlap between the NDZ (+) and NDZ (-) regions is essential to reduce the NDZ. The more the injected perturbations, the lesser the NDZ. However, this introduces additional harmonic components into the power system.

2.2.1. Asymmetrical bi-lateral reactive power perturbation

Traditionally, the reactive power perturbation employed for islanding identification is symmetric, as depicted in Figure 6(a). However, with the rise in DG penetration, the overall disturbance within the DG systems may become quite insignificant. To address this concern, the asymmetric perturbation approach can be adopted, wherein the positive and negative reactive power amplitudes differ. This ensures a consistent presence of a certain level of net reactive power within the DG system, as illustrated in Figure 6(b).

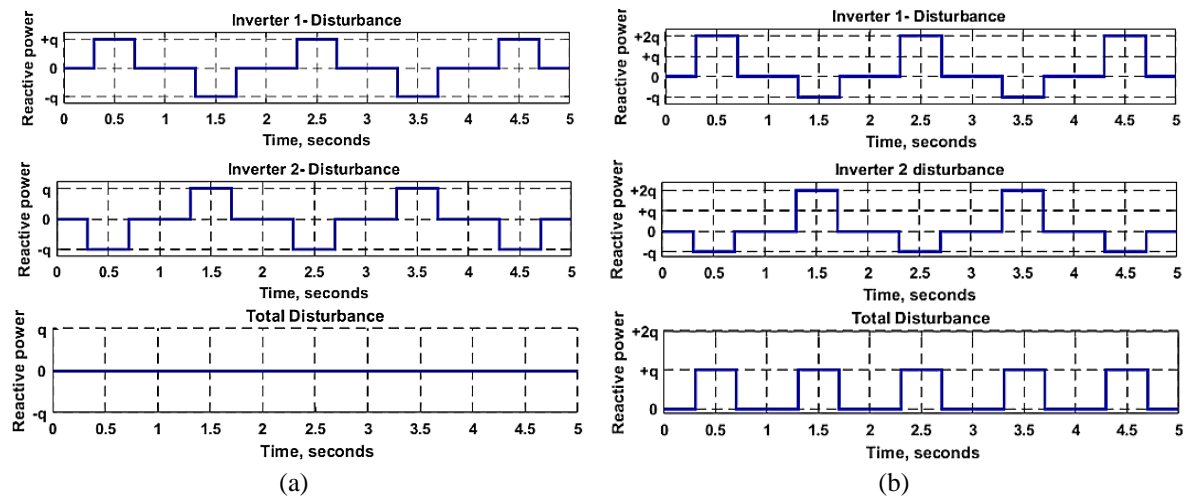


Figure 6. Bipolar reactive power injection from DG inverters in (a) symmetrical mode and (b) asymmetrical mode

3. SIMULATION RESULTS

A 50 kW DG integrated grid connected system is simulated using MATLAB/Simulink software and is presented in Figure 7. Table 2 presents the simulation parameters of the proposed system. The DG system uses a perturb and observe (P&O) MPPT algorithm. The output voltage of the boost converter is maintained at 900 V. The DG is connected to the grid at the PCC and operates with a local parallel RLC load. Figure 8 illustrates the irradiation wave.

Table 2. Test system parameters

Parameters	Ratings
DG rating	60 kVA
Load	50 kW
Q factor	2.5
f_s	5000 Hz
System voltage rating	240 V
DC bus voltage	900 V
f_0	50 Hz
$Q_{injected}$	5% of rated P
Load details	
Resistance, R	3.4445 Ω
Inductance, L	4.388 mH
Capacitance, C	2.309 mF

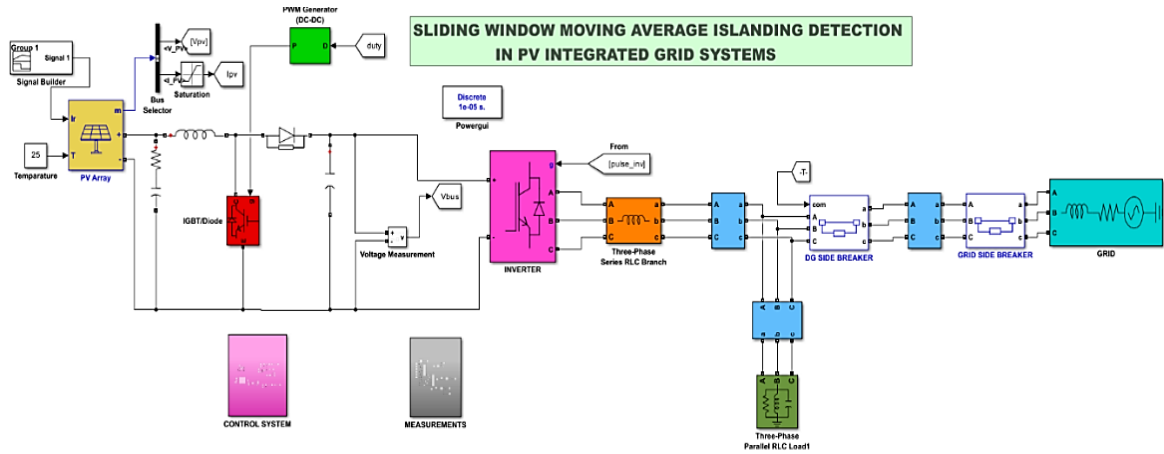


Figure 7. Simulation diagram of the proposed system

The regular variation of irradiation during day time is used for this simulation. Figure 9 presents active power output of the solar PV panel. The power output varies in accordance with the irradiation curve. Figures 10 displays the DG voltage, grid voltage and load voltage. As the DG and load are integrated to the utility grid at PCC, the three voltages are in phase to one another. Figure 11 displays the DG current, grid current, and load current which are also in phase to one another. Typically, in GIDG mode, the grid shares the deficit power. The grid share is negligible, as the load is mostly shared by the DG. During the simulation, the islanding scenario is simulated from $t=4.2$ seconds. In this specific simulation, the grid share is negligible and this load condition poses the most challenging case for islanding identification. The islanding scenario should be identified under various operating conditions and there should not be any malfunctioning under any non-islanding scenarios.

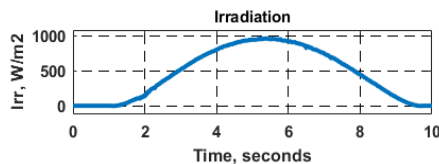


Figure 8. Irradiation curve

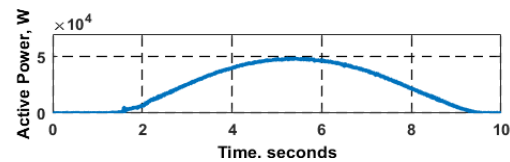


Figure 9. Active power output of PV module

3.1. Detection of islanding scenarios

3.1.1. Case 1: Large active power mismatch

In cases of substantial mismatches in active power between the DG generation and the local load demand, the proposed SWMA method effectively detects islanding scenarios. In case 1.5 kW is supplied by DG and 45 kW is supplied by grid. So there exists 90% power mismatch. As soon as islanding happens, the frequency variation occurs, therefore, the moving average and the cumulative voltage index goes above the threshold value even within the first few cycles. The result of case 1 is presented in Figure 12. From Figure 12 it is identified that the proposed method effectively identifies the islanding at $t = 4.22$ seconds following its occurrence at 4.2 seconds.

3.1.2. Case 2: Small active power mismatch

By opening the grid side breaker at $t=4.2$ seconds, the islanding operation is simulated with a minimal active power mismatch. In case 2, the DG supplies 45 kW and the grid contribute 5 kW. So, the mismatch is 10% of the rated load power. Despite the small mismatch, the cumulative voltage index has gone beyond the threshold value successfully and the proposed method accurately detects the islanding situation for this small active power mismatch. Figure 13 presents the output of case 2 where the islanding is detected at $t=4.225$ seconds. Furthermore, the ABRPP method is able to drift the cumulative voltage index at regular interval of time such as 4.5, 5.5, 6.5 seconds, which ensures the reliability of the hybrid method.

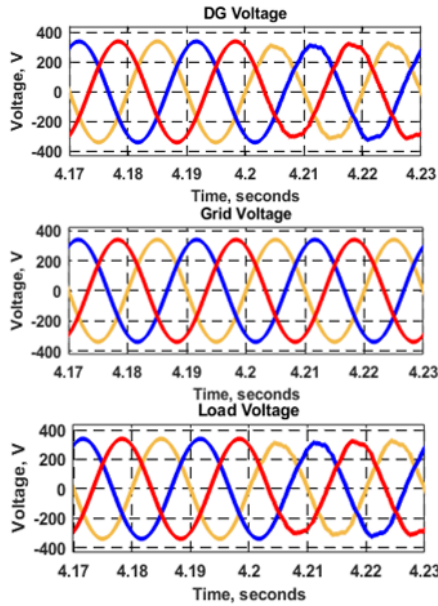


Figure 10. Three phase DG inverter voltages, grid voltages, load voltages

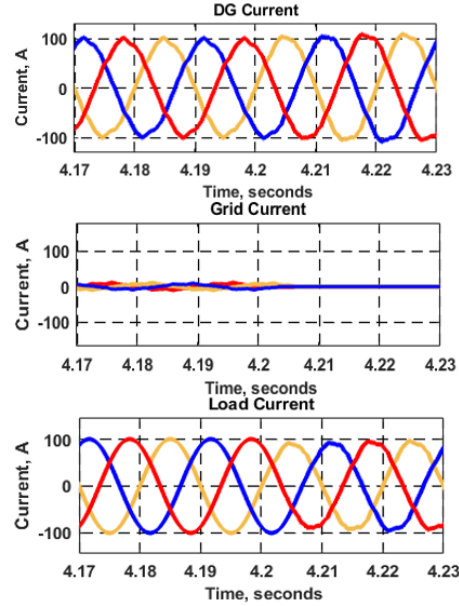


Figure 11. Three phase DG inverter currents, grid currents, load currents

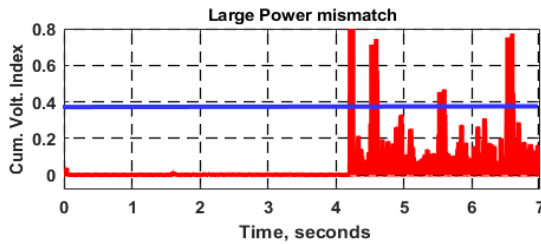


Figure 12. Cumulative voltage index for large power mismatch

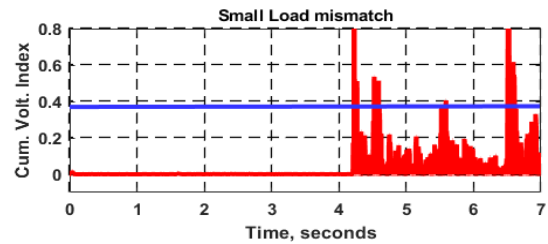


Figure 13. Cumulative voltage index for small power mismatch

3.1.3. Case 3: Different load quality factors

The quality factor is the ratio of energy stored in the reactive components of a load to that dissipated in the resistive component of an RLC circuit, per unit time. R, L, and C are determined for loads with Q_F varying from 1 to 5, as follows. The time of islanding detection is also recorded and shown in Table 3 and is also presented in Figure 14. The parallel RLC load acts as a tuned filter. The more the quality factor, the better the tuning. Therefore, at higher quality factors, the frequency adheres to the resonant frequency, 50 Hz. Hence time required for islanding detection will be more, for high quality factor loads, and the curve moves farther from the center of the radial web.

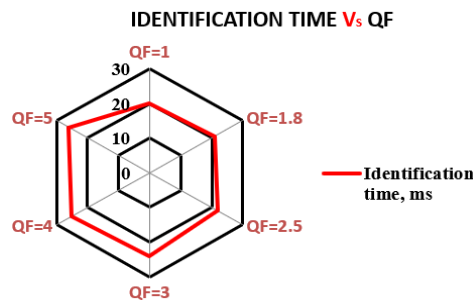


Figure 14. Detection time for various load quality factor

Table 3. Detection time for loads at different Q_F

Quality factor	Resistance	Load Inductance	Capacitance	Time of detection
1	3.4445 Ω	10.97 mH	0.9235 mF	20 mS
1.8	3.4445 Ω	6.09 mH	1.66 mF	21 mS
2.5	3.4445 Ω	4.388 mH	2.309 mF	22 mS
3	3.4445 Ω	3.657 mH	2.77 mF	24 mS
4	3.4445 Ω	2.742 mH	3.695 mF	25 mS
5	3.4445 Ω	2.194 mH	4.618 mF	26 mS

3.2. Non-islanding scenarios

3.2.1. Case 1: Switching loads in grid-tied operation

To ensure that the proposed method avoids nuisance tripping, it is essential to verify load switching under grid-connected conditions. This verification confirms that the method can handle load switching without triggering unnecessary tripping. A 25 kW (50%) load is connected at $t=3$ seconds and subsequently disconnected at $t=3.5$ seconds. The grid-tied operation shows no notable alteration in the cumulative voltage index either at the instants of load connection or disconnection. However, the cumulative voltage index has gone beyond the threshold level, when islanding occurs. The proposed method effectively identifies the islanding at $t=4.222$ seconds following its occurrence at 4.2 seconds and avoids nuisance tripping, as depicted in Figure 15.

3.2.2. Case 2: Motor load switching

At $t=3$ seconds, a 20 hp, 415 V, 50Hz, 1440 rpm induction motor is connected, and it is disconnected at $t=3.5$ seconds. The grid-connected mode experiences no substantial alteration in the cumulative voltage index during the motor connection or disconnection, ensuring the absence of nuisance tripping. However, during islanding the cumulative voltage index has shifted above the threshold value. Therefore, the proposed method effectively identifies the occurrence of islanding at $t=4.226$ seconds following its occurrence at $t=4.2$ seconds, as shown in Figure 16 and clearly avoids the nuisance tripping.

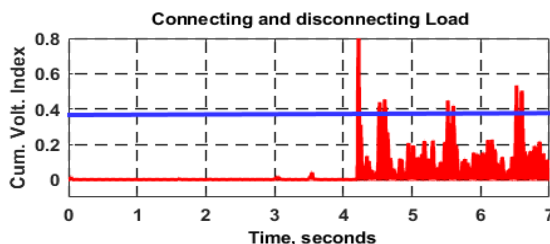


Figure 15. Cumulative voltage index during load connection

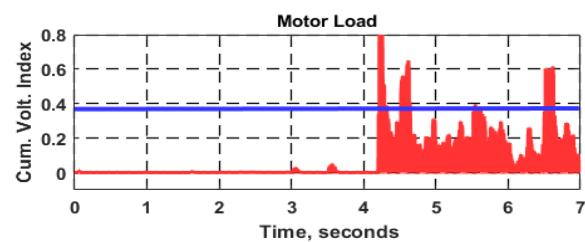


Figure 16. Cumulative voltage index during motor switching

3.2.3. Case 3: Capacitor bank switching

At $t=3$ seconds, a 25 kVAR three-phase capacitor bank is connected, and it is disconnected at $t=3.5$ seconds. During GRIDG operation, there is no significant change in the cumulative voltage index, even when the capacitor bank is connected or disconnected, ensuring the absence of nuisance tripping. However, the cumulative voltage index has gone beyond the threshold value, when the utility supply is lost. Therefore, the proposed method successfully identifies the islanding scenario, 0.22 s after it occurs at $t=4.2$ seconds, and avoids the malfunctioning, as presented in Figure 17.

3.2.4. Case 4: Non-linear load switching analysis

The GRIDG is connected to a three-phase controlled rectifier with a 25 kW load. The nonlinear load is switched in at $t=3$ seconds and disconnected at $t=3.5$ seconds. Figure 18 presents the results of cumulative voltage index during the non-linear load switching. From Figure 18 it is identified that when non-linear load is switched on or switched off, there is no significant impact on cumulative voltage index during GRIDG mode. Therefore, the proposed algorithm avoids the false tripping due to nonlinear load switching. But, as the cumulative voltage index exceeds the threshold value during islanding state, it effectively detects islanding at 4.22 seconds, following its occurrence at 4.2 seconds.

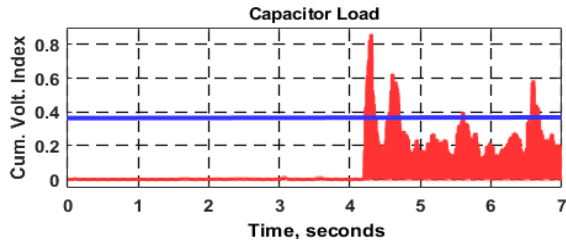


Figure 17. Cumulative voltage index during capacitor switching

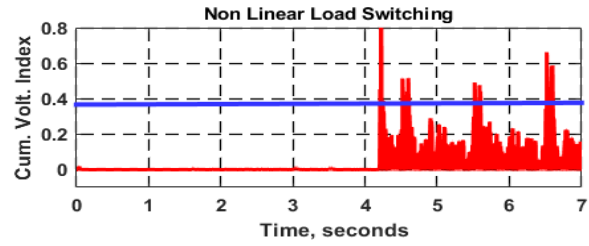


Figure 18. Cumulative voltage index during non-linear load switching

3.2.5. Case 5: Asymmetrical faults

At $t=3$ seconds, a double line to ground fault simulation is initiated, lasting for 5 cycles, and is cleared without requiring circuit breaker operation. The computation of cumulative voltage index is performed for both faulty and healthy phases. Despite cumulative voltage index having a non-zero value for A and B phase, it remains below the threshold value. Notably, there exists no false tripping, when an asymmetrical fault occurs, during GIDG operation. But when utility grid is lost, the cumulative voltage index shifts beyond the threshold limit and islanding is detected at 4.221 seconds shortly after it occurs at 4.2 s, as presented in Figure 19.

3.2.6. Case 6: Symmetrical faults

At $t=3$ seconds, a three-phase to ground fault simulation is initiated, lasting for 5 cycles, and is cleared without requiring circuit breaker operation. Though, the cumulative voltage index is more than that during an asymmetrical fault condition, it remains below the threshold value. Therefore, no nuisance tripping occurs during GIDG operation. But when utility mains are lost, the cumulative voltage index has gone beyond the threshold setting and islanding is detected at 4.221 seconds shortly after it occurs at 4.2 s, as presented in Figure 20. Figure 21 presents the comparison of the proposed method with recently developed hybrid methods. From the radial web graph, it has been observed that the developed hybrid method is very close to the center of the radial web. The nearer to the center, the lesser the detection time. Therefore, the developed method outperforms well when compared with the existing methods.

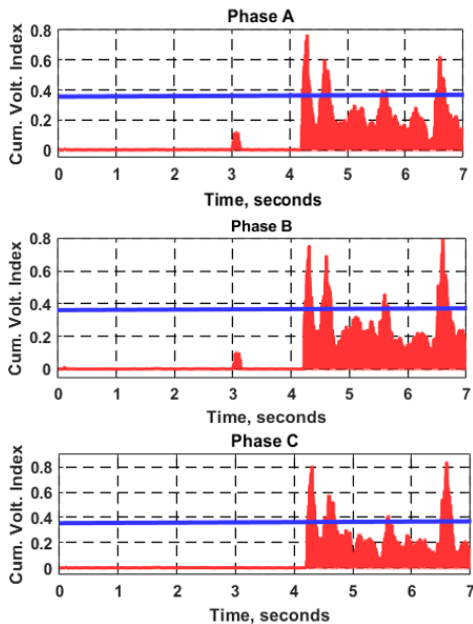


Figure 19. Cumulative voltage index during asymmetrical fault in A, B, C phases

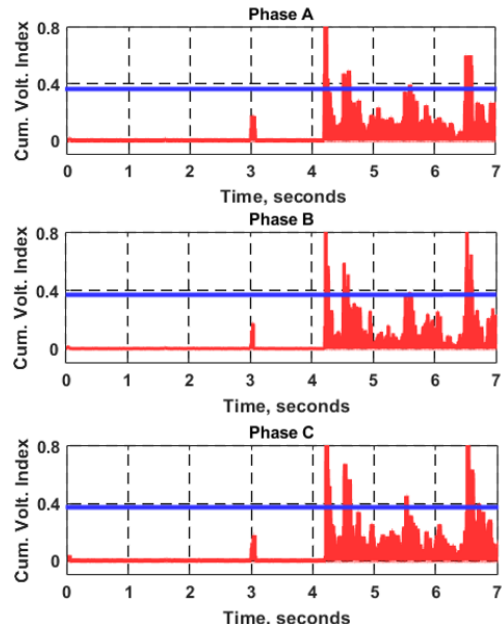


Figure 20. Cumulative voltage index during Symmetrical Fault in A, B, C phases

ISLANDING IDENTIFICATION TIME VS EXSISTING AND PROPOSED METHOD

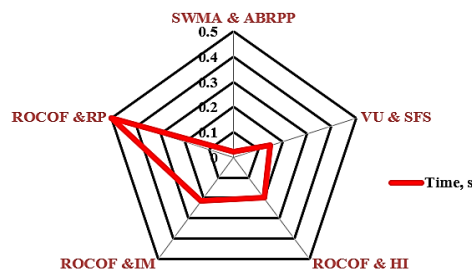


Figure 21. Detection time of various hybrid methods

4. CONCLUSION

The proposed work focuses in implementing a hybrid IIS to a GRIDG system. The validation of the proposed hybrid islanding method is conducted using the MATLAB/Simulink software. The hybrid method includes a sliding window-based moving average computation strategy which is easy to implement and asymmetrical bipolar reactive power perturbation method which is a reliable approach. The developed passive method is thoroughly tested across various power system scenarios, demonstrating satisfactory performance on its own. However, to ensure unfailing islanding identification, the asymmetrical reactive power perturbation is incorporated as a simple and reliable active method. This perturbation induces frequency deviation in the system, consequently altering the sliding window-based moving average during islanding conditions. Thus, the asymmetrical reactive power perturbation method and the sliding window-based moving average scheme work hand in hand to effectively identify the islanding scenario. Collectively, this hybrid method presents a permanent solution for islanding identification in grid-connected PV-based DGs, with potential applicability to other types of DGs as well. The response time of SWMA is as short as a few cycles, as it relies on deviation in the average value which solely related with frequency deviation. Since the SWMA method can identify islanding by its own, it need not wait until the response from active method. Thereby, the delay which usually occurs in the hybrid methods are avoided. The active method ensures the islanding detection even if SWMA fails to detect it. Therefore, the developed method works effectively under different load conditions. Moreover, the developed method poses no error while switching capacitor loads, motor loads, non-linear loads and during symmetrical and asymmetrical faults.

REFERENCES

- [1] N. K. Kasim, N. M. Obaid, H. G. Abood, R. A. Mahdi, and A. M. Humada, "Experimental study for the effect of dust cleaning on the performance of grid-tied photovoltaic solar systems," *International Journal of Electrical and Computer Engineering (IJECE)*, vol. 11, no. 1, p. 74, Feb. 2021, doi: 10.11591/ijece.v11i1.pp74-83.
- [2] T. I. Rahman, A. F. Rashid, and M. H. Rahman, "Design and development of Bi directional power meter using microcontroller," *Indonesian Journal of Electrical Engineering and Computer Science*, vol. 17, no. 3, p. 1594, Mar. 2020, doi: 10.11591/ijeecs.v17.i3.pp1594-1600.
- [3] J. Kumar, N. R. Parhyar, M. K. Panjwani, and D. Khan, "Design and performance analysis of PV grid-tied system with energy storage system," *International Journal of Electrical and Computer Engineering (IJECE)*, vol. 11, no. 2, p. 1077, Apr. 2021, doi: 10.11591/ijece.v11i2.pp1077-1085.
- [4] A. A. Adebisi, I. J. Lazarus, A. K. Saha, and E. E. Ojo, "Performance analysis of grid-tied photovoltaic system under varying weather condition and load," *International Journal of Electrical and Computer Engineering (IJECE)*, vol. 11, no. 1, p. 94, Feb. 2021, doi: 10.11591/ijece.v11i1.pp94-106.
- [5] D. Generation and E. Storage, "IEEE standard for interconnection and interoperability of distributed energy resources with associated electric power systems interfaces amendment 1: to provide more," *IEEE: Piscataway, NJ, USA*, pp. 1–16, 2020, doi: 10.1109/IEEESTD.2020.9069495.
- [6] F. Mumtaz, K. Imran, A. Abusorrah, and S. B. A. Bukhari, "An extensive overview of islanding detection strategies of active distributed generations in sustainable microgrids," *Sustainability*, vol. 15, no. 5, p. 4456, Mar. 2023, doi: 10.3390/su15054456.
- [7] J. A. Cebollero, D. Cañete, S. Martín-Arroyo, M. García-Gracia, and H. Leite, "A survey of islanding detection methods for microgrids and assessment of non-detection zones in comparison with grid codes," *Energies*, vol. 15, no. 2, p. 460, Jan. 2022, doi: 10.3390/en15020460.
- [8] M. Ropp *et al.*, "Discussion of a power line carrier communications-based anti-islanding scheme using a commercial automatic meter reading system," in *2006 IEEE 4th World Conference on Photovoltaic Energy Conference*, IEEE, 2006, pp. 2351–2354. doi: 10.1109/WCPEC.2006.279663.
- [9] J. Y. Zhang and C. M. Bush, "PMU based islanding detection to improve system operation," in *2016 IEEE Power and Energy Society General Meeting (PESGM)*, IEEE, Jul. 2016, pp. 1–5. doi: 10.1109/PESGM.2016.7741234.
- [10] H. H. Zeineldin and J. L. Kirtley, "Performance of the OVP/UVF and OFP/UFV Method With Voltage and Frequency Dependent Loads," *IEEE Transactions on Power Delivery*, vol. 24, no. 2, pp. 772–778, Apr. 2009, doi: 10.1109/TPWRD.2008.2002959.
- [11] W. Freitas, W. Xu, C. M. Affonso, and Z. Huang, "Comparative Analysis Between ROCOF and vector surge relays for distributed generation applications," *IEEE Transactions on Power Delivery*, vol. 20, no. 2, pp. 1315–1324, Apr. 2005, doi:

- 10.1109/TPWRD.2004.834869.
- [12] A. M. Nayak, M. Mishra, and B. B. Pati, "A hybrid islanding detection method considering voltage unbalance factor," in *2020 IEEE International Symposium on Sustainable Energy, Signal Processing and Cyber Security (iSSSC)*, IEEE, Dec. 2020, pp. 1–5. doi: 10.1109/iSSSC50941.2020.9358881.
 - [13] S.-I. Jang and K.-H. Kim, "An islanding detection method for distributed generations using voltage unbalance and total harmonic distortion of current," *IEEE Transactions on Power Delivery*, vol. 19, no. 2, pp. 745–752, Apr. 2004, doi: 10.1109/TPWRD.2003.822964.
 - [14] D. Reigosa, F. Briz, C. B. Charro, P. Garcia, and J. M. Guerrero, "Active islanding detection using high-frequency signal injection," *IEEE Transactions on Industry Applications*, vol. 48, no. 5, pp. 1588–1597, Sep. 2012, doi: 10.1109/TIA.2012.2209190.
 - [15] H. H. Zeineldin and S. Conti, "Sandia frequency shift parameter selection for multi-inverter systems to eliminate non-detection zone," *IET Renewable Power Generation*, vol. 5, no. 2, p. 175, 2011, doi: 10.1049/iet-rpg.2010.0096.
 - [16] M. Seyedi, S. A. Taher, B. Ganji, and J. Guerrero, "A hybrid islanding detection method based on the rates of changes in voltage and active power for the multi-inverter systems," *IEEE Transactions on Smart Grid*, vol. 12, no. 4, pp. 2800–2811, Jul. 2021, doi: 10.1109/TSG.2021.3061567.
 - [17] J. B. Jeong, H. J. Kim, S. H. Back, and K. S. Ahn, "An improved method for anti-islanding by reactive power control," in *2005 International Conference on Electrical Machines and Systems*, IEEE, 2005, pp. 965–970 Vol. 2. doi: 10.1109/ICEMS.2005.202687.
 - [18] P. Yazdkhasti and C. P. Diduch, "An islanding detection method based on measuring impedance at the point of common coupling," in *2015 IEEE 28th Canadian Conference on Electrical and Computer Engineering (CCECE)*, IEEE, May 2015, pp. 57–62. doi: 10.1109/CCECE.2015.7129160.
 - [19] N. A. Gajjar, T. Zaveri, and N. Zaveri, "Adaptive I0-LMS based algorithm for solution of power quality problems in PV-STATCOM based system," *Bulletin of Electrical Engineering and Informatics*, vol. 12, no. 2, pp. 608–618, Apr. 2023, doi: 10.11591/eei.v12i2.4174.
 - [20] V. Menon and M. H. Nehrir, "A hybrid islanding detection technique using voltage unbalance and frequency set point," *IEEE Transactions on Power Systems*, vol. 22, no. 1, pp. 442–448, Feb. 2007, doi: 10.1109/TPWRS.2006.887892.
 - [21] W.-Y. Chang, "A hybrid islanding detection method for distributed synchronous generators," in *The 2010 International Power Electronics Conference - ECCE ASIA -*, IEEE, Jun. 2010, pp. 1326–1330. doi: 10.1109/IPEC.2010.5544559.
 - [22] G. Wang, "Design consideration and performance analysis of a hybrid islanding detection method combining voltage unbalance/total harmonic distortion and bilateral reactive power variation," *CPSS Transactions on Power Electronics and Applications*, vol. 5, no. 1, pp. 86–100, Mar. 2020, doi: 10.24295/CPSSPEA.2020.00008.
 - [23] A. Rostami, H. Abdi, M. Moradi, J. Olamaei, and E. Naderi, "Islanding detection based on ROCOV and ROCORP parameters in the presence of synchronous DG applying the capacitor connection strategy," *Electric Power Components and Systems*, vol. 45, no. 3, pp. 315–330, Feb. 2017, doi: 10.1080/15325008.2016.1250842.
 - [24] J. Yin, L. Chang, and C. Diduch, "A new hybrid anti-islanding algorithm in grid connected three-phase inverter system," in *2006 37th IEEE Power Electronics Specialists Conference*, IEEE, Jun. 2006, pp. 1–7. doi: 10.1109/pesc.2006.1711989.
 - [25] A. Arif, K. Imran, Q. Cui, and Y. Weng, "Islanding detection for inverter-based distributed generation using unsupervised anomaly detection," *IEEE Access*, vol. 9, pp. 90947–90963, 2021, doi: 10.1109/ACCESS.2021.3091293.
 - [26] P. Mahat, Z. Chen, and B. Bak-Jensen, "Review on islanding operation of distribution system with distributed generation," in *2011 IEEE Power and Energy Society General Meeting*, IEEE, Jul. 2011, pp. 1–8. doi: 10.1109/PES.2011.6039299.
 - [27] K. Takeshita, O. Sakamoto, M. Maruyama, and T. Harimoto, "Consideration on voltage fluctuation caused by active method of islanding detection of photovoltaic generation," in *2018 7th International Conference on Renewable Energy Research and Applications (ICRERA)*, IEEE, Oct. 2018, pp. 1–6. doi: 10.1109/ICRERA.2018.8566972.
 - [28] G. V. Weinberg, "An invariant sliding window detection process," *IEEE Signal Processing Letters*, vol. 24, no. 7, pp. 1093–1097, Jul. 2017, doi: 10.1109/LSP.2017.2710344.
 - [29] S.-Y. Kuo and Y.-H. Chou, "Building intelligent moving average-based stock trading system using metaheuristic algorithms," *IEEE Access*, vol. 9, pp. 140383–140396, 2021, doi: 10.1109/ACCESS.2021.3119041.

BIOGRAPHIES OF AUTHORS



Praveen Raj Rajaswamy Sarojam     received his B.E degree in Electrical and Electronics Engineering from CSI Institute of technology, Thovalai, Tamil Nadu, MS University in 2002 and M.Tech. degree in Electrical Engineering from College of Engineering Trivandrum, Kerala University in 2009. His research interests include smart grids, micro grids, islanding, and electric vehicle charging systems. He can be contacted at email: praveenraj.rs@mbcet.ac.in.



Joseph Sarojini Savier     received his ME degree in Electrical Engineering from IISc Bangalore and Ph.D. degree in Electrical Engineering from IIT Kharagpur. Currently, he is working as Principal at College of Engineering Trivandrum, Kerala. His research interests include smart grids, micro-grids, distribution systems, power system protection, and energy storage. He can be contacted at email: savier_js@yahoo.com.